

## RESEARCH ARTICLE

## A theoretical analysis of single molecule protein sequencing via weak binding spectra

Samuel G. Rodrigues<sup>1,2</sup>, Adam H. Marblestone<sup>1</sup>, Edward S. Boyden<sup>1,3,4,5,6,7\*</sup>

**1** Synthetic Neurobiology Group, MIT, Cambridge, MA, United States of America, **2** Department of Physics, MIT, Cambridge, MA, United States of America, **3** McGovern Institute, MIT, Cambridge, MA, United States of America, **4** Media Lab, MIT, Cambridge, MA, United States of America, **5** Department of Biological Engineering, MIT, Cambridge, MA, United States of America, **6** Department of Brain and Cognitive Sciences, MIT, Cambridge, MA, United States of America, **7** Koch Institute, MIT, Cambridge, MA, United States of America

\* [esb@media.mit.edu](mailto:esb@media.mit.edu)

## OPEN ACCESS

**Citation:** Rodrigues SG, Marblestone AH, Boyden ES (2019) A theoretical analysis of single molecule protein sequencing via weak binding spectra. PLoS ONE 14(3): e0212868. <https://doi.org/10.1371/journal.pone.0212868>

**Editor:** Andrew C. Gill, University of Lincoln, UNITED KINGDOM

**Received:** July 27, 2018

**Accepted:** February 11, 2019

**Published:** March 28, 2019

**Copyright:** © 2019 Rodrigues et al. This is an open access article distributed under the terms of the [Creative Commons Attribution License](https://creativecommons.org/licenses/by/4.0/), which permits unrestricted use, distribution, and reproduction in any medium, provided the original author and source are credited.

**Data Availability Statement:** All relevant data are within the paper and its Supporting Information files.

**Funding:** SR acknowledges the Hertz Fellowship. ESB acknowledges NIH 1R01MH114031, John Doerr, Open Philanthropy, NIH 1R01EB024261, the HHMI-Simons Faculty Scholars Program, U. S. Army Research Laboratory and the U. S. Army Research Office under contract/grant number W911NF1510548, and NIH Director's Pioneer Award 1DP1NS087724. \*The funders had no role in

## Abstract

We propose and theoretically study an approach to massively parallel single molecule peptide sequencing, based on single molecule measurement of the kinetics of probe binding (Havranek, et al., 2013) to the N-termini of immobilized peptides. Unlike previous proposals, this method is robust to both weak and non-specific probe-target affinities, which we demonstrate by applying the method to a range of randomized affinity matrices consisting of relatively low-quality binders. This suggests a novel principle for proteomic measurement whereby highly non-optimized sets of low-affinity binders could be applicable for protein sequencing, thus shifting the burden of amino acid identification from biomolecular design to readout. Measurement of probe occupancy times, or of time-averaged fluorescence, should allow high-accuracy determination of N-terminal amino acid identity for realistic probe sets. The time-averaged fluorescence method scales well to weakly-binding probes with dissociation constants of tens or hundreds of micromolar, and bypasses photobleaching limitations associated with other fluorescence-based approaches to protein sequencing. We argue that this method could lead to an approach with single amino acid resolution and the ability to distinguish many canonical and modified amino acids, even using highly non-optimized probe sets. This readout method should expand the design space for single molecule peptide sequencing by removing constraints on the properties of the fluorescent binding probes.

## Introduction

Massively parallel DNA sequencing has revolutionized the biological sciences [2, 3], but no comparable technology exists for massively parallel sequencing of proteins. The most widely used DNA sequencing methods rely critically on the ability to locally amplify (i.e., copy) single DNA molecules—whether on a surface [4], attached to a bead [5], or anchored inside a hydrogel matrix [6]—to create a localized population of copies of the parent single DNA molecule. The copies can be probed in unison to achieve a strong, yet localized, fluorescent signal for readout via simple optics and standard cameras. For protein sequencing, on the other hand,

study design, data collection and analysis, decision to publish, or preparation of the manuscript.

**Competing interests:** The authors have declared that no competing interests exist.

there is no protein ‘copy machine’ analogous to a DNA polymerase, which could perform such localized signal amplification. Thus, protein sequencing remains truly a single molecule problem. While true single molecule DNA sequencing approaches exist [7–9], these often also rely on polymerase-based DNA copying, although direct reading of single nucleic acid molecules is beginning to become possible with nanopore approaches [10] that may be extensible to protein readout [11–13]. Thus, the development of a massively parallel protein sequencing technology may benefit from novel concepts for the readout of sequence information from single molecules.

Previously proposed approaches to massively parallel single molecule protein sequencing [14–16] utilize designs that rely on covalent chemical modification of specific amino acids along the chain. Such chain-internal tagging reactions are currently available only for a small subset of the 20 amino acids, and they have finite efficiency. Thus, such approaches would likely not be able to read the identity of every amino acid along the chain.

An alternative approach to protein sequencing [1, 17–19] is to use successive rounds of probing with N-terminal-specific amino-acid binders (NAABs) [1]. Recent studies have proposed that proteins derived from N-terminal-specific enzymes such as aminopeptidases [20], or from antibodies against the PITC-modified N-termini arising during Edman degradation [21], could be used as NAABs for protein sequencing. Yet designing or evolving highly specific, strong N-terminal binders to all 20 amino acids (and more if post-translational modifications, e.g., phosphorylation, are considered) is a challenge. Rather than attempting to improve the properties of the NAABs themselves, we will introduce a strategy—which we term “spectral sequencing”—to work around the limitations of existing NAABs and enable single molecule protein sequencing without the need to develop novel binding reagents.

Spectral sequencing measures the affinities of many low-affinity, relatively non-specific NAABs, collectively determining a “spectrum” or “profile” of affinity across binders, for each of the N-terminal amino acids. This profile is sufficient to determine the identity of the N-terminal amino acid. Thus, rather than requiring individual binders to be specific in and of themselves, we will infer a specific profile by *combining measurements of many non-specific interactions*. The spectral sequencing approach measures the single molecule binding kinetics in a massively parallel fashion, using a generalization of Points Accumulation for Imaging in Nanoscale Topography (PAINT) techniques [22, 23] to N-terminal amino acid binders. A key advantage of this technique is that it overcomes photobleaching limitations previously observed with fluorescence-based single-molecule protein sequencing methods [24].

In what follows, we first derive the capabilities of single-molecule fluorescence based measurement of probe binding kinetics as a function of probe properties and noise sources. We then apply this analysis to the problem of sequencing proteins by measuring profiles of NAAB binding kinetics. Using a range of randomized NAAB affinity matrices as well as an affinity matrix derived directly from the existing measured NAAB kinetics [1], we estimate via simulation that the kinetic measurement scheme presented here could achieve 97.5% percent accuracy in amino acid identification over a total observation period of 35 minutes, even in the presence of errors arising from instrument calibration or variation in the underlying kinetics of the binders due to the effects of non-terminal amino acids.

## Problem overview

We consider the problem in which a set of peptides is immobilized on a surface and imaged using total internal reflection fluorescence (TIRF) microscopy. The surface must be appropriately passivated to minimize nonspecific binding [19, 25–31]. Moreover, an appropriate method must be selected for anchoring peptides to the surface. We assume that the reactive

thiol group of cysteine is used to anchor peptides to the surface, but alternative methods, such as anchoring the C-terminal carboxylic acid to the surface, are also possible [24]. In all that follows, we will assume that cysteine is used to anchor the peptides to the surface, in which case the sequencing ends at the anchored cysteine.

The limited vertical extent of the evanescent excitation field of the TIRF microscope allows differential sensitivity to fluorescent molecules which are near the microscope slide surface, which allows us to detect NAABs that have bound to peptides on the surface. Existing sets of NAABs (e.g. [1]), derived from aminopeptidases or tRNA synthetases with affinities biased towards specific amino acids, have low affinity or specificity (Fig 1A), so one cannot deduce the identity of an N-terminal amino acid from the binding of a single NAAB. Instead, we propose to deduce the identity of the N terminal amino acid of a particular peptide by measuring optically the kinetics of a set of NAABs against the peptide. After observing the binding of each NAAB against the peptide, we will carry out a cycle of Edman degradation [32, 33], revealing the next amino acid along the chain as the new N-terminus, and then repeat the process. The process of observing binding kinetics with TIRF microscopy (Fig 1B and 1C) is similar to that used in Points Accumulation for Imaging of Nanoscale Topography (PAINT [22]), e.g., DNA PAINT [23]. This process produces a high-dimensional vector of kinetically-measured affinities at each cycle (Fig 1D and 1E) that can be used to infer the N-terminal amino acid.

This method, while powerful and potentially applicable for current NAABs, ultimately breaks down for probes with off-rates faster than the imaging frame rate, or for which the bound time is so short that only a small number of photons (e.g. less than 100, corresponding to  $\sim 10\%$  shot noise) is released while the probe is bound. While fast camera frame rates can be used, the system ultimately becomes limited in the achievable fluorescent signal to noise ratio, unless the measurements are averaged over long experiment times. To extend these concepts into the ultra-weak binding regime, therefore, we propose not to measure the precise binding and unbinding kinetics but rather the time-averaged luminosity of each spot, which indicates the fraction of time a probe was bound. We find that this luminosity-based measurement scheme is highly robust and compatible with short run times.

## Results

Our results are divided into three sections. We first consider the regimes of binder concentration and illumination intensity within which one would expect the proposed method to operate. We then discuss two possible methods for analyzing single molecule kinetic data. Finally, we perform simulations using the derived parameters and data analysis methods in order to estimate the sensitivity of the proposed sequencing method.

### Distinguishability of amino acids based on their NAAB binding profiles

A set of binders (NAABs) is characterized by their affinities for their targets (e.g., the 20 amino acids), which can be expressed in the form of an affinity matrix. The affinity matrix  $A$  is defined such that the  $i,j$ th entry of  $A$  is the negative log affinity of the  $i$ th binder for the  $j$ th target:

$$a_{i,j} = -\log(k_D) \quad (1)$$

where  $k_D$  is the dissociation constant (we define  $\tau_D$  as the dissociation time).

Throughout this paper, the values of the affinities encoded in the affinity matrix will be referred to as the *reference* values, to distinguish them from the *measured* values obtained in the experiment and from the *true* values, which may depend on environmental conditions but

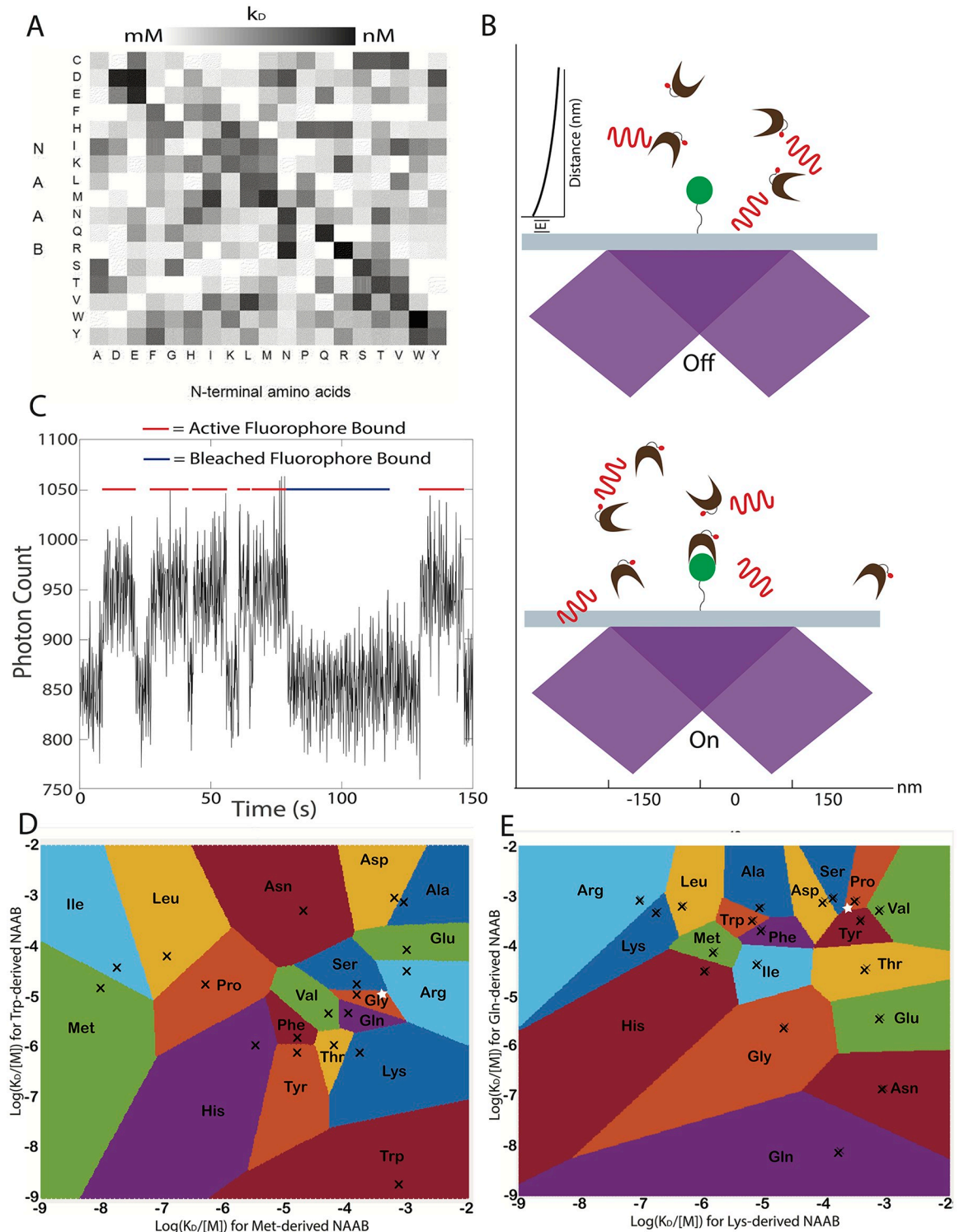


**Fig 1. Identifying amino acids from kinetic measurements.** **A** Example affinity matrix for a set of NAABs. The affinities of each of the 17 NAABs are shown for all 19 amino acids excluding cysteine, which is used to anchor the peptides to the surface. Reproduced from [1]. **B** In the proposed measurement scheme, the target (green disk) is attached to a glass slide and is observed using TIRF microscopy. NAAB binders (brown clefts) bearing fluorophores (red dots) are excited by a TIRF beam (purple) and generate fluorescent photon emissions (red waves). **C** When a fluorophore is bound, there is an increase in fluorescence in the spot containing the target. Photobleaching of the fluorophore is indistinguishable from unbinding events, so it is important to use a dye that is robust against

photobleaching. Plot shows an illustrative stochastic kinetics simulation incorporating Poisson shot noise of photon emission. A relatively strong binder is shown solely for purposes of illustration. In practice, the method relies on many measurements performed on weak binders. **D** The plot shows the result of a proposed kinetic measurement on an N-terminal amino acid using only two NAABs. The affinity of each N-terminal amino acid (black Xs, excluding cysteine) for the methionine-targeting and tryptophan-targeting NAABs are shown as a scatterplot, with the affinity for the met-targeting NAAB on the x axis and the affinity for the Trp-targeting NAAB on the y axis. Upon measuring the affinities for these NAABs against an unknown target undergoing sequencing, the unknown target can be identified with the amino acid with expected vector of affinities closest in the two-dimensional Euclidean space (higher-dimensional in a full experiment) to the measured affinity. The colored regions correspond to the regions within which a measured multi-NAAB affinity vector would be assigned to a given amino acid. As an example, a pair of measurements yielding the white star in **D** would identify the target as glycine. **E** The affinities of the glutamine and lysine targeting NAABs are shown for each of the amino acids. Some amino acids that are practically indistinguishable using the Met and Trp NAABs are easily distinguished using the Gln and Lys NAABs. As an example, if the same target amino acid described in **D** were measured with only the Gln and Lys NAABs, yielding the white star, we would identify the target as proline. However, combining these measurements with those for the white star in **D** with Met and Trp NAABs, we see that the true identity of the target is serine. Thus, the higher dimensional measurement of the amino acid using many different NAABs allows disambiguation of the amino acid identity.

<https://doi.org/10.1371/journal.pone.0212868.g001>

which are not known by the experimenter; the reference values are known and will be used in our computational process of identifying amino acids. As shown in **Appendix A**, we estimate that it would be possible to determine the identities of the N terminal amino acids from affinity measurements with 99% accuracy, provided that the affinity measurements occur according to a distribution centered on the reference value with standard deviation no greater than 64% of the mean.

## Model parameters

In order to evaluate the feasibility of the kinetic measurement strategy, we designed a model to simulate the observation of NAAB binding and unbinding from a peptide target, using TIRF microscopy. In evaluating the kinetic measurement strategy, we must make assumptions about the relevant photophysical parameters.

1. The rate  $R$  of photons from a single fluorophore captured by the detector, per second. This is a product of numerous parameters specific to the experimental implementation, including the collection efficiency of the optical setup, the illumination intensity, the quantum efficiency of the fluorophore, and the quantum efficiency of the detector. We use realistic values in the range of 10,000 photons per second [23, 34–36].
2. The mean number  $N_q$  of photons that a fluorophore can emit before it photobleaches. Realistic numbers on the order of  $N_q \sim 10^7$  have been reported for Atto647N [23].
3. The pixel size. We will assume that peptides are anchored to the surface sparsely enough so that there is at most one peptide per pixel. We will further assume that each pixel collects light from a cylindrical region 300 nm in diameter and 100 nm in depth, corresponding to visible TIRF illumination. It is useful to bear in mind that a free fluorophore occupation number of  $n_{\text{free}} \approx 1$  in every cylinder with diameter 300 nm and height 100 nm corresponds to a molar density of 235 nM.
4. The background level. Each pixel collects some amount of background light. We draw a distinction between transient emission sources (such as diffusing fluorophores) and constant sources of background photons, such as autofluorescence and excitation of fluorophores in the bulk by first- and higher-order beams. Transient emission sources are modeled, but we decline to model autofluorescence and bulk excitation, because previous studies have shown that the contribution of those sources are small compared to the fluorescence of fluorophores excited by the zeroth order beam [23].



- The free NAAB concentration,  $n_{free}$ . The choice of  $n_{free}$  is up to the experimenter and may be chosen differently for different NAABs. It will need to be optimized to maximize the dynamic range of the  $k_D$  readout experiment.

### Methods of data analysis

A single-molecule experiment using TIRF yields a time series such as that shown in Fig 2A. We now discuss the two primary options for extracting the kinetics from this data and the experimental conditions that are optimal for each scheme, given the constraints discussed above.

**Occupancy measurements.** The first measurement, used commonly in the field of single-molecule kinetics [23, 37], relies on detecting changes in the occupancy state of the target. The measurement scheme is depicted schematically in Fig 2B. This measurement is performed “along the time axis,” in the sense that it relies on temporal information—when probes bind

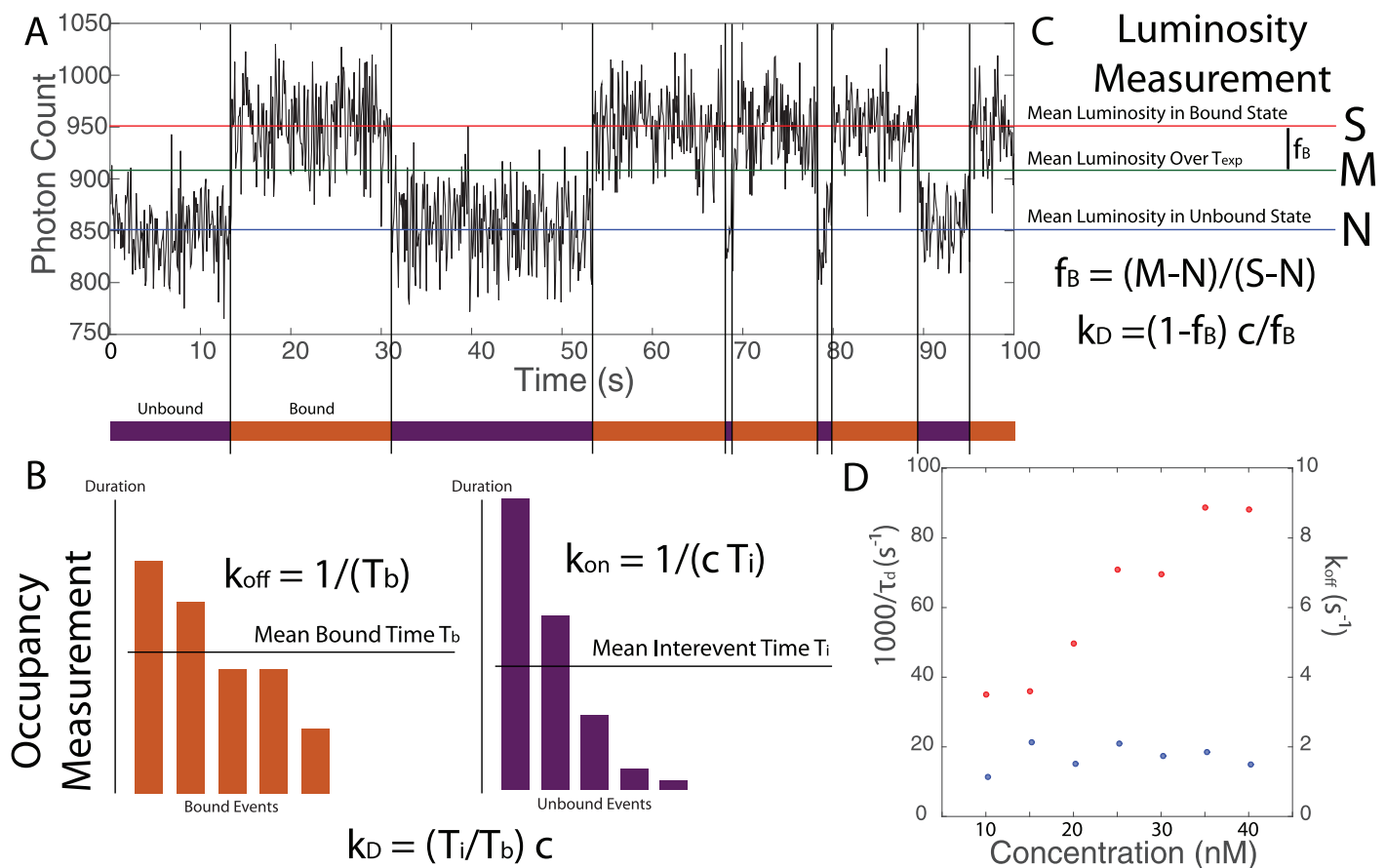


**Fig 2. Two types of affinity measurements using TIRF microscopy.** **A** A measurement performed using the proposed scheme yields a fluorescence intensity trace where periods of high intensity correspond to the target being bound and periods of low intensity correspond to the target being free. The affinity of a binder against the target may then be determined in two ways, either via occupancy measurements or via luminosity measurements. **B** An occupancy measurement is performed “along the time axis,” by calculating  $k_{on}$  from the average time between binding events, and  $k_{off}$  from the average length of binding events. **C** On the other hand, a luminosity measurement is performed “along the brightness axis,” by calculating  $k_D$  directly from the average luminosity of the target over the whole observation period. **D** We validated our simulation by applying occupancy measurements to determine  $k_{on}$  and  $k_{off}$  from simulated data. The parameters used here were identical to those used in the production of Fig 2a in [23]. See text for symbol definitions.

<https://doi.org/10.1371/journal.pone.0212868.g002>

and unbind—and is relatively insensitive to analog luminosity information beyond that needed to make these digital determinations.

In this method, the parameters of interest are the free NAAB concentration  $n_{\text{free}}$  and the frame rate,  $f = 1/\tau_{\text{obs}}$ . The upper limit on the dynamic range of this method is set by the frame rate, i.e.,

$$\tau_{\text{obs}} \ll 1/k_{\text{off}}. \tag{2}$$

On the other hand, the lower bound on the dynamic range is set by the duration of the experiment  $T_{\text{exp}}$ , via the requirement that

$$T_{\text{exp}} \gg 1/k_{\text{off}}, \tag{3}$$

so that unbinding events can be observed, and also that

$$T_{\text{exp}} \gg 1/(k_{\text{on}}c), \tag{4}$$

so binding events can be observed. For a value of  $k_{\text{on}}$  between  $10^5 \text{ M}^{-1} \text{ s}^{-1}$  and  $10^6 \text{ M}^{-1} \text{ s}^{-1}$  (e.g. [23, 38]) and a concentration on the order of 100 nM, this requirement implies that an experiment time of at least 100 seconds is necessary in order to see several binding events with high probability. In addition, we will choose  $f = 100 \text{ Hz}$  for this measurement modality, which then implies a dynamic range of roughly 5 orders of magnitude in  $k_{\text{off}}$ . The values of  $k_{\text{off}}$  that can be discerned are also constrained by photobleaching and by the background. Specifically, if  $R$  is the rate of photon detection,  $N_q$  is the mean number of detected photons emitted by the fluorophore before bleaching, and  $B$  is the mean rate of background photon detection (due to camera noise, autofluorescence, etc.), then we also have

$$R/B \gg k_{\text{off}} \gg R/N_q. \tag{5}$$

The value of  $k_D$  is determined in this modality as follows. If the binding and unbinding events may be identified, then one may determine the average binding time  $T_b$  and the average time between binding events  $T_i$ , which we will refer to as the inter-event time. If photobleaching may be neglected, then we have

$$k_{\text{off}} = \frac{1}{T_b}, \tag{6}$$

and

$$k_{\text{on}} = \frac{1}{T_i c}, \tag{7}$$

where  $c$  is the free binder concentration. Thus,

$$k_D = \frac{T_i}{T_b} c. \tag{8}$$

Additionally, if the on-rate  $k_{\text{on}}$  is known, then it is possible to determine  $k_{\text{off}}$  even in the presence of photobleaching. (See Appendix C for details.)

**Luminosity measurements.** An alternative to the occupancy-time measurements described above involves deducing  $k_D$  directly from the fraction  $f_B$  of time that the target is bound by a probe. This quantity may in turn be deduced from the average luminosity of the spot containing the free binder over the period of observation, as depicted in Fig 2C. Whereas occupancy measurements are performed “along the time axis,” neglecting luminosity

information, luminosity measurements are performed “along the luminosity axis,” neglecting temporal information about the series of binding and unbinding events. Because it does not attempt to track individual binding and unbinding events, this method is particularly suited to measurements of weak binders performed at high background concentrations, where binding and unbinding events may occur faster than the camera frame rate. Moreover, this method relies on each NAAB of a given type having approximately the same brightness, which could be achieved using a high-efficiency method for monovalently labeling the NAAB N- or C-terminus [39, 40].

If the target is bound a fraction  $f_B$  of the time, then the dissociation constant is given by

$$k_D = \frac{1 - f_B}{f_B} c, \quad (9)$$

where  $c$  is the background binder concentration. We denote by  $S$  the average brightness of the spot when a fluorescent binder is attached to the target, and by  $N$  the average brightness of the spot when the target is free. Neglecting photobleaching, the average brightness of the spot over the whole experiment is given by

$$M = f_B S + (1 - f_B) N. \quad (10)$$

If  $S$  and  $N$  are known, then  $f_B$  may thus be deduced directly from the measured photon rate  $M$  averaged over the entire experiment, via

$$f_B = \frac{M - N}{S - N}. \quad (11)$$

$S$  and  $N$  can be measured directly for example by anchoring NAABs sparsely to a surface and measuring the brightness of the resulting puncta (to deduce  $S$ ), or puncta-free regions (to measure  $N$ ).

One significant advantage of this method is that the observation period  $\tau_{\text{obs}}$  can be chosen to be arbitrarily long by averaging the photon counts of many successive frames (i.e., we have  $\tau_{\text{obs}} = T_{\text{exp}}$ ). In practice, we will use  $\tau_{\text{obs}} = 100$  s. With this value, we can use a relatively high concentration of  $2 \mu\text{M}$  (corresponding to  $n_{\text{free}} \gg 1$ ) and a relatively low emission rate of  $R = 10^3 \text{ s}^{-1}$ . The choice of a high NAAB concentration and low illumination intensity increases the dynamic range of the measurement scheme, by increasing the sensitivity both to small values of  $k_D$ , where photobleaching might be an issue, and to high values of  $k_D$ , where observation of binding events may be an issue. However, unlike in the case of occupancy measurements, there is no way to account for photobleaching, if it occurs. Nonetheless, we do not expect photobleaching to have a significant impact on our results, since most of the NAABs have fairly high off-rates [1, 20].

## Simulations

In order to determine whether the TIRF measurement scheme described above can be used to identify single amino acids on the N-termini of surface-anchored peptides, we simulated N-terminal amino acid identification experiments.

We first used a specific NAAB affinity matrix given in [1]. Importantly, random affinity matrices (see Appendix E) generated by permuting the values of the NAAB affinity matrix perform similarly well in residue-calling simulations. To generate the random affinity matrices with statistics matching the statistics of the NAAB affinity matrix, each matrix element was chosen by randomly sampling values from the NAAB affinity matrix of [1], without replacement. The simulations described here can therefore be assumed to apply to general ensembles



of N-terminal binders with affinity value statistics similar to those displayed by these existing NAABs.

In the simulations, there is assumed to be one free target in the volume analyzed, which is a cylinder of diameter 300 nm and height 100 nm as discussed above. Thus, we assume that peptides are arrayed sparsely enough on the surface that there is at most one peptide per diffraction-limited spot. The simulation considers each frame of the camera in succession, and models the number of photons registered at the camera. At the start of the simulation, or as soon as the target becomes free, a time  $T_{\text{free}}$  is drawn from an exponential distribution with mean  $1/(k_{\text{on}}c)$ , where  $c$  is the concentration of binders. Once a time equal to  $T_{\text{free}}$  has passed, the binder is considered occupied, and a time  $T_{\text{bound}}$  is drawn from an exponential distribution with mean  $1/k_{\text{off}}$ . In addition, upon binding, a time  $T_{\text{photobleach}}$  is drawn from an exponential distribution with mean  $N_q/R$ , where  $N_q$  is the number of photons seen by the detector on average before the fluorophore bleaches and  $R$  is the number of photons seen at the detector by a single fluorophore per second. For a dye like Atto 647N, we use  $N_q = 1.2 \times 10^7$  [23]. If the time  $T_{\text{photobleach}}$  is less than the time  $T_{\text{bound}}$ , the fluorophore ceases to emit photons after time  $T_{\text{photobleach}}$ . Within a given frame, the simulation tracks binding, unbinding, and photobleaching events, and computes the number of signal photons detected by the camera by drawing from a Poisson distribution with mean  $RT_{\text{on}}$ , where  $R$  is the single fluorophore photon rate and  $T_{\text{on}}$  is the amount of time during the frame in which an unbleached fluorophore was attached to the target.

In addition to background photons, the dominant contribution to noise in the simulation is expected to come from fluorophores attached to free binders that enter and leave the observation field [37]. At the end of each frame, the simulation draws the number of free binders that enter the observation field during the frame from a Poisson distribution with mean  $n_{\text{free}}/f$ , where  $f$  is the frame rate and  $n_{\text{free}}$  is the free binder occupation number of the frame. For each binder that enters the observation field, we draw a dwell time  $t$  from an exponential distribution with mean  $\tau_{\text{dwell}}$  as calculated in Eq (27) from diffusion theory (see Appendix B), and a total photon contribution from a Poisson distribution with mean  $Rt$ . Finally, we calculate the detector shot noise from a Gaussian distribution with mean  $p$  and standard deviation equal to  $0.1p$ .

**Validation of the simulation pipeline.** To validate the simulations, we reproduced the DNA PAINT kinetics data collected by [23] using the parameters reported in that paper. There, values of  $k_{\text{on}} \sim 2.2 \times 10^6 \text{ M}^{-1} \text{ s}^{-1}$  and  $k_{\text{off}} \sim 1.8 \text{ s}^{-1}$  were reported. Although the photon rate was not directly reported in that paper, other papers using similar laser intensities and fluorophores reported photon rates on the order of  $R \sim 10000 \text{ s}^{-1}$  [34–36], so we used this value. From our simulated data, we were able to reproduce the measured off- and on-rates, as shown in Fig 2D.

## Measurements of $k_D$

We next compared the ability of occupancy and luminosity measurements to determine the dissociation constant  $k_D$  of binders for the target.

**Occupancy measurements.** We performed 100 simulations of occupancy measurements for each of five different values of  $k_{\text{on}}$  between  $10^4 \text{ M}^{-1} \text{ s}^{-1}$  and  $10^6 \text{ M}^{-1} \text{ s}^{-1}$ , which is consistent with standard values observed for antibodies [38], and for each of five different values of  $k_D$  between 100  $\mu\text{M}$  and 10 nM. We assumed a frame-rate of 100 Hz, detector read noise of  $1 \text{ e}^-$ , and a single-fluorophore detection rate of  $10^5 \text{ s}^{-1}$ . The NAAB concentration was 300 nM, and the observation time was  $T_{\text{exp}} = 100 \text{ s}$ .

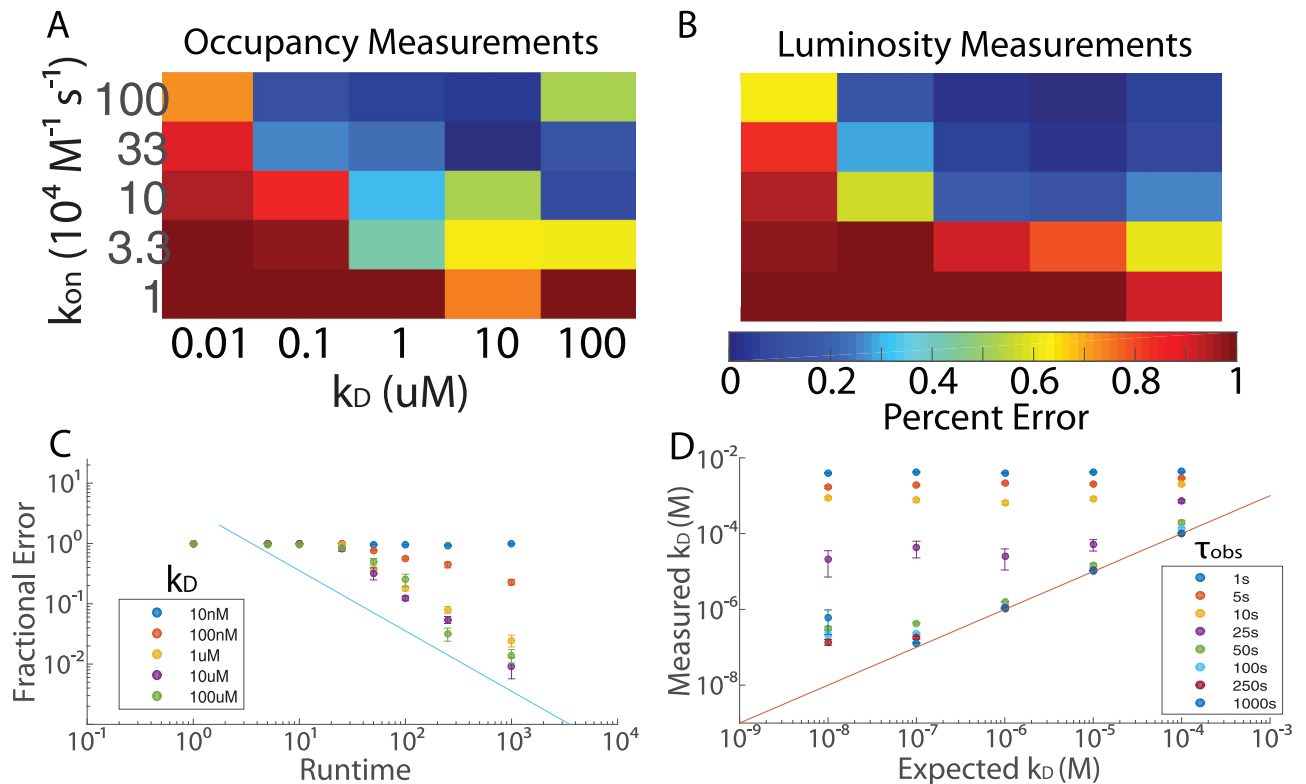


**Fig 3. Two types of affinity measurements using TIRF microscopy.** **A** The accuracies of occupation measurements of  $k_D$  are shown as a function of  $k_D$  and  $k_{on}$  for the simulation described in the text, with  $T_{exp} = 100$  s. These measurements achieve high accuracy for  $k_{on} \geq 10^4 \text{ M}^{-1} \text{ s}^{-1}$  and  $k_{off} \ll 100 \text{ s}^{-1}$ . For values of  $k_{off}$  on the order of  $100 \text{ s}^{-1}$  (upper right-hand corner), the accuracy deteriorates significantly. **B** The accuracies of luminosity measurements of  $k_D$  are shown as a function of  $k_D$  and  $k_{on}$ . These measurements achieve high accuracy for  $k_{on} \geq 10^5 \text{ M}^{-1} \text{ s}^{-1}$  and  $k_D \geq 100 \text{ nm}$ . The heat map shown gives the fractional errors as a function of  $k_D$  and  $k_{on}$  for the simulation described in the text, with  $T_{exp} = 100$  s. In contrast to occupation measurements, the accuracy of luminosity measurements does not deteriorate for very high values of  $k_{off}$ . **C** For luminosity measurements only, the mean fractional error in the measured value of  $k_D$  is plotted as a function of the observation time for five different values of  $k_D$ . The line  $y = 1/x$  is plotted as a guide to the eye. For  $k_D = 10 \text{ nm}$  and  $k_D = 100 \text{ nm}$ , the effects of photobleaching are evident at longer runtimes. **D** Also, for luminosity measurements only, the measured value of  $k_D$  is plotted as a function of the actual value of  $k_D$  for 8 different values of the runtime. The performance of the algorithm improves dramatically for  $\tau_{obs} > 25$  s. The line  $y = x$  is plotted as a guide to the eye. Error bars in C, D denote standard error over 100 trials.

<https://doi.org/10.1371/journal.pone.0212868.g003>

In order to analyze the data, we ran a control simulation in which  $k_{on}$  was set to 0, so that no NAABs bound to the target. In practice, this calibration could be performed by observing a spot that does not have a target. From this, we calculated the mean and standard deviation of the noise on a per-frame basis. We then identified binding and unbinding events as follows. First, we identified all frames in which the photon count was more than 2 standard deviations above the noise mean. These frames will be referred to as “on” frames, whereas all other frames will be referred to as “off” frames. If three such “on” frames occurred in a row, the event was identified as a binding event. The binding event was considered to continue until at least two “off”-frames in a row were observed. Once all the binding and unbinding events were identified, the average inter-event time and the average binding time were calculated, and from these the kinetics were deduced (Fig 2A).

The accuracy of the  $k_D$  measurements was found to improve with increasing  $k_{on}$ , and to improve with increasing  $k_D$  for values of  $k_{off}$  below  $10 \text{ s}^{-1}$  (Fig 3A). For values of  $k_{off}$  significantly above  $10 \text{ s}^{-1}$ , it was no longer possible to distinguish individual binding and unbinding events from noise (Fig 3A, upper right-hand corner). Moreover, for values of  $k_{on}$  below  $10^5$

$\text{M}^{-1} \text{s}^{-1}$ , the condition  $T_{\text{exp}} \gg 1/(k_{\text{on}} c)$  was no longer satisfied. Finally, for very small values of  $k_D$ , photobleaching limited the accuracy of the analysis. For  $k_{\text{on}} > 10^5 \text{M}^{-1} \text{s}^{-1}$  and  $k_{\text{off}} \sim 10 \text{s}^{-1}$ , it was possible to obtain the correct value of  $k_D$  to within approximately 5 – 10%. However, the accuracy deteriorated sharply for combinations of  $k_{\text{on}}$  and  $k_{\text{off}}$  deviating from these ideal conditions.

**Luminosity measurements.** We then simulated luminosity measurements of  $k_D$  using comparable parameters. Because these measurements depend only on the average luminosity over the entire experiment, the entire experiment was lumped into a single camera frame. In practice, however, the same results can be obtained by averaging over the photon counts of multiple frames. The photon detection rate was set to  $R = 1000 \text{s}^{-1}$ , and the free binder concentration was set to  $2 \mu\text{M}$ . The photon rate of the off-state was determined first by running the simulation with the value of  $k_{\text{on}}$  set to 0. The photon rate in the on-state was then determined by running the simulation with the value of  $k_{\text{on}}$  set to  $10^{10} \text{M}^{-1} \text{s}^{-1}$ , and the value of  $k_D$  set to  $10^{-20}$ . Because the exposure time used in this experiment is very long compared to the dwell time of free binders in the observation field, it was assumed that all free binders that enter the observation field emit a number of photons equal to  $R\tau_{\text{dwell}}$  (i.e., the noise was taken to be approximately Poissonian), which substantially reduces the computational complexity of the algorithm. Once the average luminosity over the experiment was determined, the value of  $f_B$  was deduced.

For observation times shorter than 50 s, the analysis sometimes returns values of  $f_B$  arbitrarily close to or greater than 1 or arbitrarily close to or less than 0. This can happen as a consequence of statistical error in the luminosity measurements, even in the absence of systematic error. For this reason, in order to avoid negative or outlandishly large values of  $k_D$  from compromising the analysis, we chose the maximum value of  $f_B$  to be equal to the value expected when  $k_D = 1 \text{ nM}$ , and we chose the minimum value of  $f_B$  to be equal to the value obtained when  $k_D = 10 \text{ mM}$ . Any values of  $f_B$  outside of this range were adjusted to the maximum or minimum value, appropriately.

In order to enable comparison to the occupancy measurements, the simulation was run 100 times for each of five values of  $k_{\text{on}}$  between  $10^4 \text{M}^{-1} \text{s}^{-1}$  and  $10^6 \text{M}^{-1} \text{s}^{-1}$  and for each of five values of  $k_D$  between  $100 \mu\text{M}$  and  $10 \text{ nM}$ . The accuracy was found to be comparable to that obtained in the occupancy experiments (Fig 3A), except that the accuracy did not deteriorate for very high values of  $k_{\text{off}}$  (Fig 3B, upper right-hand corner). For values of  $k_{\text{on}}$  on the order of (or greater than)  $10^5 \text{M}^{-1} \text{s}^{-1}$  and values of  $k_D$  greater than  $1 \mu\text{M}$ ,  $k_D$  could easily be determined to within the accuracy condition required by Eq (18).

To ascertain the effect of  $\tau_{\text{obs}}$  on the accuracy, the simulation was run 100 times for each of the same 25 combinations of  $k_{\text{on}}$  and  $k_{\text{off}}$ , with 8 different values of  $\tau_{\text{obs}}$  between 1 s and 1000 s and a free binder population of  $2 \mu\text{M}$  (Fig 3C). As expected, the accuracy was found to undergo a sharp transition when  $\tau_{\text{obs}}$  was on the order of 25 s, corresponding to  $1/(k_{\text{on}}c) \ll \tau_{\text{obs}}$ . For values of  $\tau_{\text{obs}} > 25 \text{ s}$  and values of  $k_D$  greater than  $1 \mu\text{M}$ , the error in the measurement of  $k_D$  decreased like  $1/\tau_{\text{obs}}$  (Fig 3C). For observation times greater than 25 s, the value of  $k_D$  could be calculated with standard deviation less than 64% of the mean for values of  $k_D$  on the order of or greater than  $1 \mu\text{M}$ , although photobleaching leads to saturation and significant losses of accuracy for smaller values of  $k_D$  (Fig 3D).

Separately, to ascertain the effect of the free binder concentration on the accuracy, the simulation was run 1000 times on each of the same 25 combinations of  $k_{\text{on}}$  and  $k_D$ , with  $\tau_{\text{obs}} = 50 \text{ s}$  at seven different values of the concentration between  $10 \text{ nM}$  and  $5 \mu\text{M}$ . For values of  $k_{\text{on}}$  such that  $\tau_{\text{obs}} \gg 1/(k_{\text{on}}c)$ , the effect of increasing  $k_{\text{on}}$  was found to be similar to the effect of increasing  $\tau_{\text{obs}}$  (data not shown).

### Identifying amino acids

Because standard deviations in  $k_D$  below 64% of the mean could consistently be achieved in the luminosity measurements across a broad range of values of  $k_{on}$  and  $k_D$ , it is reasonable to expect that luminosity measurements of NAAB binding kinetics with the affinity matrix in Fig 1A could allow for the identification of amino acids at the single molecule level. We thus simulated an experiment, using the luminosity measurement paradigm, in which a peptide with an unknown amino acid is attached to a surface, and is observed successively in multiple baths, each containing a single kind of fluorescent NAAB.

**Simulation of systematic errors.** Two kinds of systematic error may confound identification of amino acids. The first kind of error, which we refer to as kinetic error, refers to the case in which the actual dissociation constant for a particular NAAB-amino acid pair is different from the expected value. This may arise due to issues such as the secondary structure or the identities of non-terminal amino acids. To simulate this, for each NAAB, the effective dissociation constant  $\tilde{k}_D$  for the NAAB-amino acid pair was drawn from a normal distribution centered on the reference value  $k_D$ , with standard deviation equal to  $\sigma_K k_D$ , where  $\sigma_K$  parametrizes the effect of non-terminal amino acids and other environmental factors on the dissociation constant.

In addition, luminosity measurements are also sensitive to error in the calibration of the measurement apparatus, for example if the brightness of the bright and dark states is not known exactly. We refer to this kind of error as calibration error. The bright and dark states  $S$  and  $N$  could likely be calibrated by doping in labeled reference peptides to the sample to be sequenced. Still, there may be some error in the measurements of  $S$  and  $N$ . To simulate this kind of error, the true calibration levels  $S$  and  $N$  were first determined as the luminosity of the bound and unbound states. The measured calibration levels  $\tilde{S}$  and  $\tilde{N}$  were then determined by drawing from a normal distribution with mean equal to  $S$  and  $N$  and with standard deviation equal to  $\sigma_C S$  and  $\sigma_C N$ , respectively. The values of  $\sigma_K$  and  $\sigma_C$  will be given below in percentages. For a discussion of computational strategies for coping with calibration error, see Appendix D.

**Amino acid identification.** In this simulation, amino acids were randomly chosen from a uniform distribution. Binders were added to the solution at a concentration of  $1 \mu\text{M}$  and the photon detection rate was set to  $1000 \text{ s}^{-1}$ . For each NAAB, effective values of the dissociation constant  $\tilde{k}_D$ , the on-rate  $\tilde{k}_{on}$ , the effective brightness  $\tilde{R}$ , and the calibration levels  $\tilde{S}$  and  $\tilde{N}$  were determined for the NAAB-amino acid pair. The spot containing the NAAB was then observed over a period of time  $\tau_{obs}$ , which ranged from 50 to 500 seconds, and the total number of photons observed was stored. This process was repeated for each NAAB, generating a vector  $\vec{M}$  of observed photon counts.

Analysis was performed by comparing the measured photon counts to the photon counts that would have been expected for each amino acid, as described above. For each NAAB-amino acid pair, the expected photon count was calculated from the NAAB concentration  $c$ , the reference value of  $k_D$  and the measured calibration level  $\tilde{S}$  and  $\tilde{N}$ , via

$$\vec{E} = \frac{c}{c + k_D} \tilde{S} + \left(1 - \frac{c}{c + k_D}\right) \tilde{N}. \tag{12}$$

The resulting expected photon counts were then assembled into a matrix  $W$ , such that the  $(i, j)$ th element of  $W$  is the photon count that one would have expected on the measurement of the  $i$ th NAAB if the target were the  $j$ th amino acid, given the calibration levels  $\tilde{S}$  and  $\tilde{N}$ . Finally, the amino acid identity  $I_{aa}$  was determined by minimizing the norm between the vector of

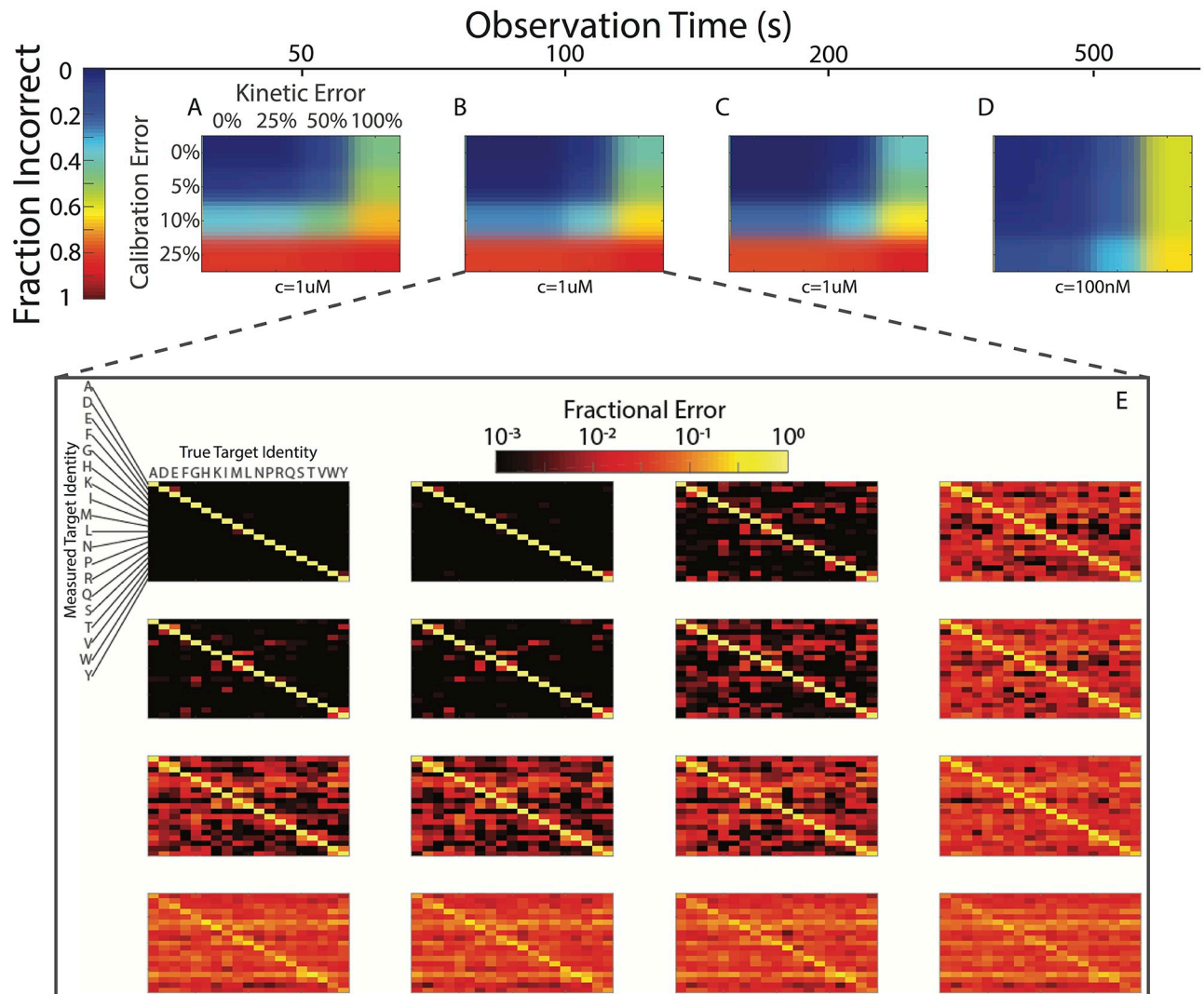


**Fig 4. Identification of amino acids is robust against systematic error.** The fraction of amino acids incorrectly identified is plotted as a function of  $\tau_{\text{obs}}$  for four different values of the systematic calibration error  $\sigma_C$  and four different values of the systematic kinetic error  $\sigma_K$  (as described in the text). **A** In the absence of systematic error, measurements with  $\tau_{\text{obs}} = 50$  s result in correct amino acid identification more than 98% of the time. For 25% error in  $k_D$ , the accuracy drops to 97.5%, and if 5% calibration error is added, it drops further to 92%. More than 5% systematic error in the calibration leads to very significant numbers of mistakes in amino acid identification. **B** With  $\tau_{\text{obs}} = 100$  s, an accuracy of 97.5% was obtained for 25% error in  $k_D$  and 5% error in the calibration. Axes for B, C, and D are the same as in A. **C** Increasing  $\tau_{\text{obs}}$  beyond 100 s at the same binder concentration leads to diminishing improvements in the accuracy. **D** The sensitivity to calibration error could be substantially reduced by decreasing the concentration of free binders to 100 nM. However, this decreased concentration necessitates a longer runtime. **E** For  $\tau_{\text{obs}} = 100$  s, plots are shown for each value of  $\sigma_C$  and  $\sigma_K$ , depicting the probability that a given target amino acid (on the horizontal axis) was assigned a particular identity (on the vertical axis). Off-diagonal elements correspond to errors.

<https://doi.org/10.1371/journal.pone.0212868.g004>

observed photon counts  $\vec{M}$  and the columns of  $W$ , i.e.,

$$I_{\text{aa}} = \operatorname{argmin}_k \|\vec{M} - \vec{w}_k\|, \tag{13}$$

where  $\vec{w}_k$  is the  $k$ th column of  $W$ .

In Fig 4A–4C, the accuracy with which amino acids can be identified is shown as a function of the observation time and the systematic error, for a 1  $\mu\text{M}$  free binder concentration. In the absence of systematic error, amino acids could be identified with greater than 99% accuracy

after a 50 s observation. Moreover, the experiment also showed robustness against kinetic error up to the 25% level, with progressive deterioration in the measurement accuracy observed for values of  $\sigma_K$  above 25%. Calibration error was found to have the most substantial effect on the accuracy, with calibration errors on the order of 10% reducing the achievable accuracy below 90% even for an observation time of 250 s. The effects of calibration error on the accuracy could be substantially reduced by reducing the concentration of free binders (Fig 4D), which has the effect of increasing the gap between the  $S$  and  $N$ . However, in order to preserve the requirement that  $T_{\text{exp}} \gg 1/(k_{\text{on}}c)$ , it is necessary to increase the experiment length by a similar factor. (For this reason, a free NAAB concentration of 1  $\mu\text{M}$  was used, rather than 2  $\mu\text{M}$  as used above.) Moreover, this improvement comes at the cost of increased sensitivity to systematic error in  $k_D$ . If the calibration error can be kept below 5%, and if the systematic error in the kinetics can be kept below 25%, then our simulations indicate that it would be possible to identify amino acids with greater than 97.5% accuracy over an observation window of 100 s.

### Application to randomized affinity matrices

In order to determine whether the protein sequencing method proposed here is limited to the specific affinity matrix given in [1], we generated affinity matrices with comparable binding statistics by randomly shuffling the  $k_D$  values in the NAAB affinity matrix. For 100 such random affinity matrices, we then performed identical simulations as in Fig 4E, assuming 5% calibration error and 25% kinetic error. To calculate the overall error rate for a given matrix, we summed the frequencies of incorrect residue calls (the off-diagonal elements of the matrices in Fig 4E). The overall error rate for the NAAB affinity matrix, calculated in this way, is 0.0124, and the distribution of error rates across the random matrices is shown in Fig 5. Only one randomly generated affinity matrix had an error rate lower than the NAAB error rate. Nonetheless, it is clear that most affinity matrices with affinity statistics similar to the NAABs [1] would

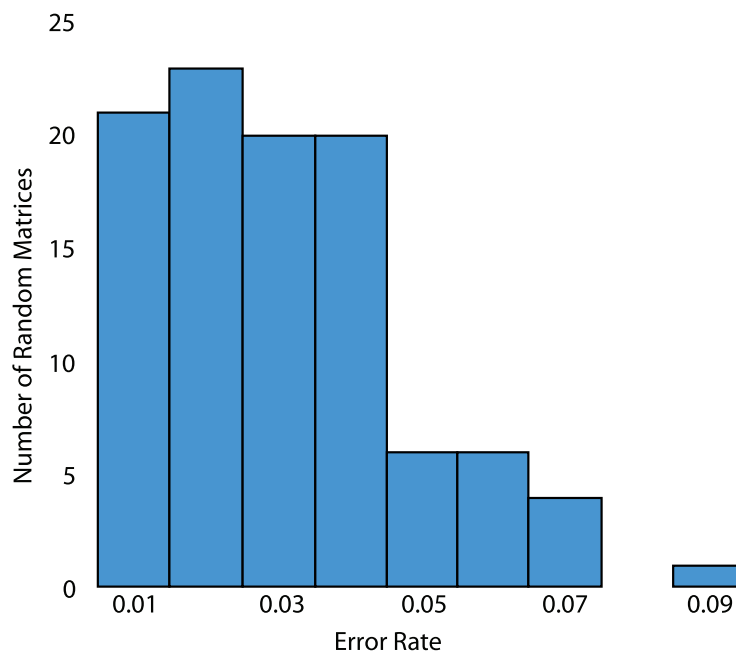


**Fig 5. Overall error rates for 100 random affinity matrices.** A histogram of the overall error rate, calculated as the sum of incorrect residue calls divided by the total number of residue calls over 10000 trials, is plotted for 100 random affinity matrices.

<https://doi.org/10.1371/journal.pone.0212868.g005>



yield errors in the range of 1%-4%, and thus the sequencing method described here is generalizable to a range of similar N-terminal amino acid binders.

## Discussion

The calculations and simulations discussed above indicate that if the measurement apparatus can be calibrated with an accuracy of 5%, and if the reference values of  $k_D$  can be kept within 25% of the true values, it is theoretically possible to determine the identity of an N-terminal amino acid with greater than 97.5% accuracy by measuring the kinetics of the NAABs against the target amino acid. Crucially,  $k_D$  can be inferred just from the time-averaged local concentration of NAABs within the observation field, and thus the measurement can be performed at relatively high background binder concentrations, because it does not rely on being able to distinguish individual binding and unbinding events.

## Primary uncertainties

Three primary uncertainties exist regarding the validity of the simulations performed here. Firstly, our simulation did not incorporate the effects of non-specific binding of NAABs to the surface. However, non-specific binding will simply increase the level of background fluorescence, and numerous recent single-molecule imaging studies have demonstrated surface passivation techniques that minimize nonspecific background [23, 41].

Secondly, the sequencing will take place in non-denaturing buffers, as is necessary for the NAABs. We anticipate that small, surface-anchored peptides derived by cleaving proteins will be accessible for NAAB binding, as has been shown previously, for example in the case of bio-layer interferometry [1]. However, some peptides may not be sequenceable in this method due to secondary structures or other idiosyncrasies.

In addition, some uncertainty exists surrounding the value of  $N_q$  for the organic dyes of interest to us, with values between  $10^5$  and  $10^7$  being reported [23, 42]. However, we expect our method to be relatively robust to photobleaching due to the relatively low affinity and high off-rates of most of the NAABs. Moreover, it is possible that more photostable indicators such as quantum dots could be used in place of organic dyes. Note that with any labeling scheme, there will be some concentration of “dark NAABs” that are not labeled. We do not expect this to be a major issue for the detection scheme provided the total NAAB concentration is less than the dissociation constant (i.e., as long as the target is free most of the time). However, if this is an issue, several other strategies are available to ensure high-efficiency labeling of NAABs, for example expressing the NAABs as fusions to a fluorescent protein, or to a peptide tag or protein (e.g. the SNAP tag) that can be used to link the NAABs to small molecule fluorophores with high efficiency. Moreover, a high concentration of dark NAABs can always be compensated for by reducing the total NAAB concentration and increasing the measurement duration. Nonetheless, the concentrations reported for the simulations above should be regarded as the concentrations of successfully labeled “bright NAABs.”

## Calibration error

The luminosity measurement scheme is particularly sensitive to calibration error. This is because the brightness of puncta in the luminosity measurement scheme is used to infer the fraction  $f_B$  of the time that the NAAB is bound, and when that fraction is close to 1 or close to 0, then small systematic errors in estimating  $f_B$  can contribute to large errors in estimating  $k_D$ . A more robust scheme might be to use the *relative* luminosity of different NAABs, which would then account for effects due to the structure of the peptide (e.g. aromatic residues such as tryptophan might contribute to quenching) and due to local variations in surface

passivation. One straightforward way to do this would be to normalize the luminosities to the luminosity of a particular high-affinity NAAB.

### Parallelization

We anticipate that the approaches discussed here could be parallelized in a way reminiscent of next-generation nucleic acid sequencing technologies, allowing for massively parallel protein sequencing with single-molecule resolution. In the ideal case, if a 64 megapixel camera were used with one target per pixel, we would have the ability to observe the binding kinetics of NAABs against approximately  $10^7$  protein fragments simultaneously. With an observation time of 100 seconds per amino acid-NAAB pair, this corresponds to approximately 35 minutes of observation time per amino acid, or 5 days to identify a protein fragment of 200 amino acids in length. As the method is scaled up, the imaging time will come to dominate over the time needed for the fluidic and chemical steps. For example, one flow cell could be imaged while Edman degradation proceeds on a different flowcell. More generally, because imaging requires photon collection through a magnification system, and data transfer to a computer, it is likely to be largely serial, or parallel only up to the number of parallel cameras, whereas fluidic wash and reaction steps can occur in parallel over an entire large surface. Thus in the limit of acquiring data from large flow cells the chemical cycle time of the Edman degradation steps is negligible compared to the imaging time. On average, therefore, the sequencing method as a whole would have a throughput of approximately 20 proteins per second per 64-megapixel camera and its associated imaging setup.

However, the throughput of the device could be improved dramatically if the readout mechanism were electrical, rather than optical. CMOS-compatible field-effect transistors have been developed as sensors for biological molecules [43–46]. Moreover, electrical sequencing of DNA has been accomplished using ion semiconductor sequencing [47]. Most recently, CMOS-compatible carbon nanotube FETs have been shown to detect DNA hybridization kinetics with better than 10 ms time resolution [48, 49]. Similar CMOS-compatible devices have been adapted to the detection of protein concentrations via immunodetection [50]. These systems have the added benefit that they sense from a much smaller volume than TIRF does (sometimes as small as  $\sim 10$  cubic nanometers [49]), substantially reducing the impact of noise on the measurement. A single 5 inch silicon wafer covered in transistor sensors at a density of 16 transistors per square micron would be capable of sequencing  $10^{12}$  proteins simultaneously, corresponding to an average throughput of 2,000,000 proteins per second on a single wafer, or one mammalian cell every 7 minutes. Such an approach could make use of dedicated integration circuitry to compute the average NAAB occupancy at the hardware level, greatly simplifying data acquisition and processing. Moreover, if the devices were made CMOS-compatible, they could be produced in bulk, greatly improving scalability. If the intrinsic contrast provided by the NAABs is insufficient for measurements with FETs, the NAABs can be further engineered to have greater electrical contrast, for example by conjugating them on the C-terminus to an electrically salient protein such as ferritin. A combination of electrical and optical readouts may also be desirable. Recently, CMOS-compatible single-photon avalanche diode imaging systems have been developed that are capable of detecting the presence of fluorophores on a surface without optics [51].

Finally, although the use of TIRF microscopy in the case studied here restricts the proposed approach to operate close to a reflecting surface, the use of thin sections or alternative microscopies could potentially allow such protein sequencing methods to operate *in-situ* inside intact cells or tissues.

## Conclusion

We have shown that single molecule protein sequencing is possible using low-affinity, low-specificity binding reagents and single molecule fluorescent detection. Achieving a high-quality single molecule surface chemistry and TIRF measurement setup will be a challenge, but if this can be achieved, our results show that a wide range of binding reagent families should be adaptable to single molecule protein sequencing.

## 1 Appendix A

Due to stochasticity, noise, and context-dependence (e.g. sequence-dependence) of the NAAB-amino acid interactions, a measurement performed on the  $k$ th target will yield an approximation  $\vec{w}$  to the reference affinity vector  $\vec{v}_k$ . If we assume that the distribution according to which these measurements occur is Gaussian, then we can obtain a simple criterion for determining whether two N terminal amino acids will be distinguishable on the basis of affinity measurements made using a particular set of NAABs. We denote by  $\sigma_j^{(i)}$  the standard deviation of the measurements made with NAAB  $i$  against amino acid  $j$ . For each amino acid, we may define a sphere of radius  $\rho_j$ , centered on the vector  $\vec{v}_j$ , which surrounds that amino acid in affinity space. Here,

$$\rho_j = 3 \max_i \frac{\sigma_j^{(i)}}{K_j^{(i)}}, \tag{14}$$

where  $K_j^{(i)}$  is the dissociation constant for the binding of the  $i$ th NAAB to the  $j$ th amino acid.

N-terminal amino acids will be identifiable with 99.9% certainty provided that there is no overlap in affinity-space between the  $j$  spheres of radius  $\rho_j$ . To determine whether there is such an overlap, we must consider the distance metric

$$D \equiv \min_{i,j \neq i} \left\| \frac{\vec{v}_i - \vec{v}_j}{\vec{v}_i} \right\|, \tag{15}$$

where the division is applied element-wise. In order to assign affinity measurements to the correct reference affinity 99.9% of the time, it is sufficient (but not necessary) to have

$$\max_{i,j \neq i} (\rho_i + \rho_j) \leq D. \tag{16}$$

Using Eq (14), it is then also sufficient to have

$$6 \max_{i,k \neq i} \frac{\sigma_k^{(i)}}{K_k^{(i)}} \leq D. \tag{17}$$

For the specific case of the NAAB affinity matrix, we find that  $D = 3.84$ . Thus, in order to ensure that the amino acids can be correctly identified 99.9% of the time, we must have

$$\max_{i,k \neq i} \frac{\sigma_k^i}{K_k^{(i)}} \leq 0.64, \tag{18}$$

or, equivalently, the standard deviation of the  $k_D$  measurements must be no greater than 64% of the mean.

## 2 Appendix B

Under the assumption of Poissonian noise, the photon rates in the bound and unbound states are given by

$$\lambda_f = R\tau_{\text{obs}}n_{\text{free}} \tag{19}$$

and

$$\lambda_b = R\tau_{\text{obs}}(n_{\text{free}} + 1) \tag{20}$$

respectively. In order to be able to distinguish the bound state from the unbound state, it is clear that we must have

$$\lambda_f + 3\sqrt{\lambda_f} \leq \lambda_b - 3\sqrt{\lambda_b}. \tag{21}$$

Because  $\lambda_b > \lambda_f$ , we may replace the standard deviation  $\sqrt{\lambda_f}$  on the left-hand side by the standard deviation  $\sqrt{\lambda_b}$ , obtaining

$$\lambda_f \leq \lambda_b - 6\sqrt{\lambda_b}. \tag{22}$$

Hence,

$$R\tau_{\text{obs}} \geq 6\sqrt{R\tau_{\text{obs}}(n_{\text{free}} + 1)}. \tag{23}$$

We find the final requirement:

$$n_{\text{free}} \leq \frac{R\tau_{\text{obs}}}{36} - 1. \tag{24}$$

Rephrased as a condition on the concentration of the binder, we find

$$c \leq \frac{\frac{R\tau_{\text{obs}}}{36} - 1}{1000N_A V}, \tag{25}$$

or

$$R\tau_{\text{obs}} \geq 36(1 + n_{\text{free}}). \tag{26}$$

If  $n_{\text{free}} \leq 1$ , then the assumption of Poissonian noise is invalidated because the emission of successive photons is not independent (it depends on the presence of fluorophores in the observation field). The assumption of Poissonian noise may also be invalidated if the frame rate is comparable to the rate at which fluorophores enter and leave the observation field. In either case, to correctly simulate the noise, one must draw the number of free binders that enter the observation field during a given frame from a Poisson distribution with mean  $n_{\text{free}} \tau_{\text{obs}}/\tau_{\text{dwell}}$ , where  $\tau_{\text{dwell}}$  is the amount of time each binder spends in the observation field on average. The average dwell time of free binders in a region of thickness  $\Delta x$  may be calculated as

$$\tau_{\text{dwell}} = (\Delta x)^2/D, \tag{27}$$

where  $D$  is the diffusion constant [23]. For a small protein in water, we have  $D \sim 10^{10} \text{ m}^2 \text{ s}^{-1}$ . Taking  $\Delta x = 100 \text{ nm}$ , we find that free binders will dwell on average  $\tau_{\text{dwell}} = 100 \text{ }\mu\text{s}$  within the imaging plane.

Once the number of binders entering the observation field during the frame has been determined, one must draw the length of time  $t$  that each binder remains in the frame from an exponential distribution with mean  $\tau_{\text{dwell}}$ . Finally, for each binder, one must draw the number of photons emitted by that binder from a Poisson distribution with mean  $Rt$ . When the number of free binders is small, the resulting noise will differ significantly from Poisson noise due to the exponential distribution over dwell times. In our simulations, the long tail of the exponential distribution tends to significantly increase the difficulty of distinguishing transient binding and unbinding events, compared to simple Poisson noise (data not shown).

### 3 Appendix C

One advantage of occupancy measurements is that if  $k_{\text{on}}$  is known, then  $k_{\text{off}}$  may be determined even in the presence of photobleaching. To do so, we note that  $T_i$  and  $T_b$  are independent variables that depend on  $k_{\text{off}}$ ,  $k_{\text{on}}$ , and  $N_q$ . In the above analysis, we assumed that  $N_q$  was infinite, so that quenching could be neglected. If  $N_q$  is finite, however, then the true expressions for  $T_i$  and  $T_b$  are given by

$$T_b = \frac{1}{k_{\text{off}} + R/N_q} \tag{28}$$

and

$$T_i = \underbrace{\left( \frac{1}{k_{\text{off}}} - T_b \right)}_{\text{target occupied}} + \underbrace{\frac{1}{k_{\text{on}}c}}_{\text{target unoccupied}} \tag{29}$$

The first term in Eq (29) is the average time the target spends occupied by a quenched fluorophore, while the second term is the average time the target spends unoccupied between unbinding and binding events. Hence, if  $k_{\text{on}}$  is known, then  $k_{\text{off}}$  and  $N_q$  may be determined from  $T_b$  and  $T_i$ .

### 4 Appendix D

In contrast to occupancy measurements, luminosity measurements are sensitive to error in the calibration of the measurement apparatus. Calibration error arises from a combination of systematic differences in the brightness of the on- and off-states, which may result if different NAABs have different numbers of fluorophores on average, and from systematic error in the measurement of the brightnesses of the on- and off-states. Systematic variation in the brightnesses of the fluorophores can be overcome by calibrating the device prior to each measurement (as discussed below). In general, however, systematic error in the measurement of  $S$  and  $N$  significantly disrupts attempts to determine the absolute value of  $k_D$  due to divergences in the derivative of  $k_D$  as  $M$  approaches  $N$ . Hence, for weak binders in particular, infinitesimal changes in the calibration level can lead to divergent changes in the measured value of  $k_D$ . For this reason, if the goal of the measurement is to determine the absolute value of  $k_D$ , it is essential that the concentration be chosen such that the value of  $M$  to be measured lies close to  $S$ , i.e., such that the concentration  $c$  is close to or greater than  $k_D$ . If  $k_D$  is large or unknown, however, this requirement may not be achievable.

In our case, however, we are interested not in determining the absolute value of  $k_D$ , but rather in determining the identity of a target (N-terminal amino acid) from the binding affinities of many binders (NAABs). In this case, one may significantly reduce the effects of calibration error by using the reference values of  $k_D$  to calculate the expected photon rate  $E$  from the

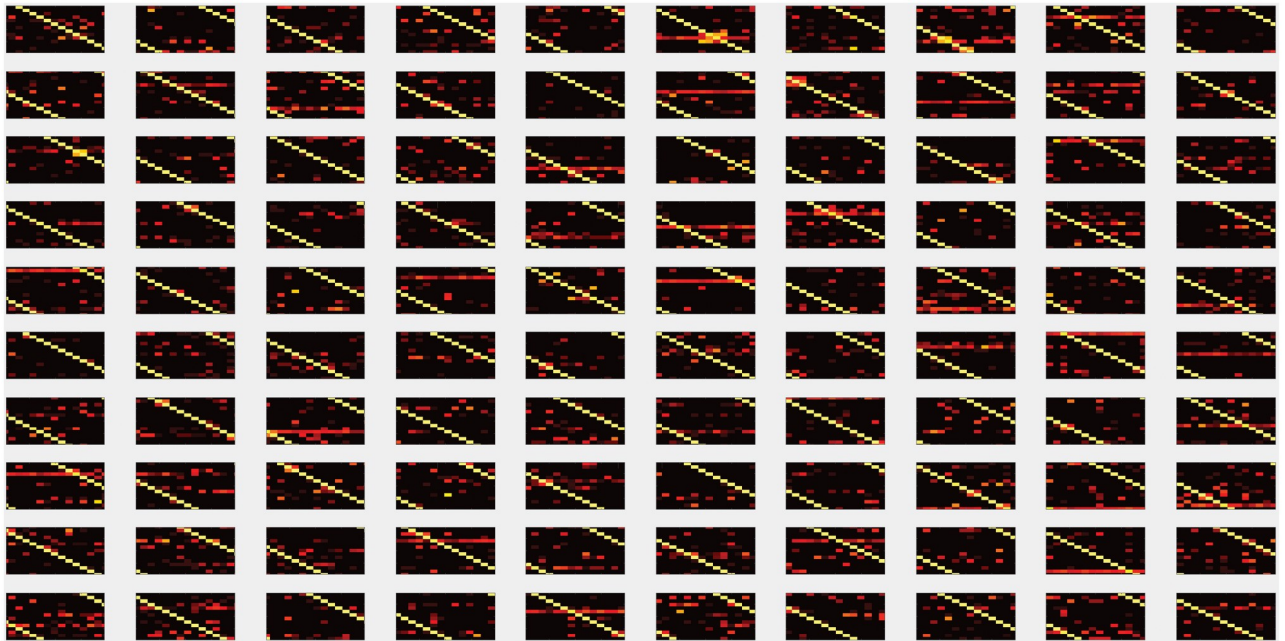


**Fig 6. Accuracies for amino acid calling obtained for 100 random affinity matrices in simulations.** 100 random affinity matrices were generated by randomly shuffling the entries of the NAAB affinity matrix. For each resulting matrix, we simulated 10000 amino acid calls, with 5% calibration error and 0.25% kinetic error. The resulting accuracy matrices are presented here. The scale and axes for each matrix are identical to those in Fig 4E.

<https://doi.org/10.1371/journal.pone.0212868.g006>

brightnesses of the on- and off-states, for each of the possible target identities. After having performed the measurement with all 17 binders, one is left with a vector  $\vec{M}$  of the photon rates measured for each binder, and a set of vectors  $\vec{E}_k$ , the  $k$ th of which is the vector of photon rates that one would have expected to measure if the target were of type  $k$ . The identity of the target is then determined by minimizing the norm of  $\vec{M} - \vec{E}_k$  over  $k$ . The key difference here is that because one compares the expected photon rates to the measured photon rates, one avoids the nonlinearities inherent in calculating the measured dissociation constant from the measured photon rate.

## 5 Appendix E

Fig 6 shows the full set of accuracy matrices determined by simulation for 100 random affinity matrices.

### Supporting information

**S1 Data.** A supporting data file is included in .mat format containing the NAAB affinities digitized from [1].

(MAT)

### Acknowledgments

We thank Andrew Payne, Jim Havranek and Jeff Nivala for helpful discussions. SR acknowledges funding from the Fannie and John Hertz Fellowship. ESB acknowledges funding from NIH 1R01MH114031, John Doerr, Open Philanthropy, NIH 1R01EB024261, the HHMI-Simons Faculty Scholars Program, U.S. Army Research Laboratory and the U. S. Army



Research Office under contract/grant number W911NF1510548, and NIH Director's Pioneer Award 1DP1NS087724.

## Author Contributions

**Conceptualization:** Samuel G. Rodriques, Adam H. Marblestone, Edward S. Boyden.

**Formal analysis:** Samuel G. Rodriques, Adam H. Marblestone.

**Funding acquisition:** Edward S. Boyden.

**Investigation:** Samuel G. Rodriques.

**Methodology:** Samuel G. Rodriques, Edward S. Boyden.

**Software:** Samuel G. Rodriques.

**Supervision:** Adam H. Marblestone, Edward S. Boyden.

**Visualization:** Samuel G. Rodriques.

**Writing – original draft:** Samuel G. Rodriques, Adam H. Marblestone.

**Writing – review & editing:** Samuel G. Rodriques, Adam H. Marblestone, Edward S. Boyden.

## References

1. Havranek JJ, Borgo B, inventors; Washington University in St Louis, assignee. Molecules and methods for iterative polypeptide analysis and processing. US20140273004A1; 2013. Available from: <https://patents.google.com/patent/US20140273004A1/en>.
2. Shendure J, Mitra RD, Varma C, Church GM. Advanced sequencing technologies: methods and goals. *Nature Reviews Genetics*. 2004; 5(5):335–344. <https://doi.org/10.1038/nrg1325> PMID: 15143316
3. Shendure J, Aiden EL. The expanding scope of DNA sequencing. *Nature biotechnology*. 2012; 30(11):1084–1094. <https://doi.org/10.1038/nbt.2421> PMID: 23138308
4. Bentley DR, Balasubramanian S, Swerdlow HP, Smith GP, Milton J, Brown CG, et al. Accurate whole human genome sequencing using reversible terminator chemistry. *Nature*. 2008; 456(7218):53–59. <https://doi.org/10.1038/nature07517> PMID: 18987734
5. Brenner S, Johnson M, Bridgham J, Golda G, Lloyd DH, Johnson D, et al. Gene expression analysis by massively parallel signature sequencing (MPSS) on microbead arrays. *Nature biotechnology*. 2000; 18(6):630–634. <https://doi.org/10.1038/76469> PMID: 10835600
6. Mitra RD, Shendure J, Olejnik J, Church GM, et al. Fluorescent in situ sequencing on polymerase colonies. *Analytical biochemistry*. 2003; 320(1):55–65. [https://doi.org/10.1016/S0003-2697\(03\)00291-4](https://doi.org/10.1016/S0003-2697(03)00291-4) PMID: 12895469
7. Levene MJ, Korfach J, Turner SW, Foquet M, Craighead HG, Webb WW. Zero-mode waveguides for single-molecule analysis at high concentrations. *Science*. 2003; 299(5607):682–686. <https://doi.org/10.1126/science.1079700> PMID: 12560545
8. Braslavsky I, Hebert B, Kartalov E, Quake SR. Sequence information can be obtained from single DNA molecules. *Proceedings of the National Academy of Sciences*. 2003; 100(7):3960–3964. <https://doi.org/10.1073/pnas.0230489100>
9. Fuller CW, Kumar S, Porel M, Chien M, Bibillo A, Stranges PB, et al. Real-time single-molecule electronic DNA sequencing by synthesis using polymer-tagged nucleotides on a nanopore array. *Proceedings of the National Academy of Sciences*. 2016; 113(19):5233–5238. <https://doi.org/10.1073/pnas.1601782113>
10. Garalde DR, Snell EA, Jachimowicz D, Sipos B, Lloyd JH, Bruce M, et al. Highly parallel direct RNA sequencing on an array of nanopores. *Nature methods*. 2018;. <https://doi.org/10.1038/nmeth.4577> PMID: 29334379
11. Nivala J, Marks DB, Akeson M. Unfoldase-mediated protein translocation through an  $\alpha$ -hemolysin nanopore. *Nature biotechnology*. 2013; 31(3):247. <https://doi.org/10.1038/nbt.2503> PMID: 23376966
12. Kolmogorov M, Kennedy E, Dong Z, Timp G, Pevzner PA. Single-molecule protein identification by sub-nanopore sensors. *PLoS computational biology*. 2017; 13(5):e1005356. <https://doi.org/10.1371/journal.pcbi.1005356> PMID: 28486472

13. Sampath G. A digital approach to protein identification and quantity estimation using tandem nano-pores, peptidases, and database search. *bioRxiv*. 2015; p. 024158.
14. Swaminathan J, Boulgakov AA, Marcotte EM. A theoretical justification for single molecule peptide sequencing. *bioRxiv*. 2014; p. 010587.
15. Yao Y, Docter M, Van Ginkel J, de Ridder D, Joo C. Single-molecule protein sequencing through fingerprinting: computational assessment. *Physical biology*. 2015; 12(5):055003. <https://doi.org/10.1088/1478-3975/12/5/055003> PMID: 26266455
16. van Ginkel J, Filius M, Szczepaniak M, Tulinski P, Meyer AS, Joo C. Single-Molecule Peptide Fingerprinting. *Biophysical Journal*. 2017; 112(3):471a. <https://doi.org/10.1016/j.bpj.2016.11.2529>
17. Borgo B, Havranek JJ. Computer-aided Design of a Catalyst for Edman Degradation Utilizing Substrate-Assisted Catalysis. *Protein Science*. 2014;.
18. Borgo B. Strategies for Computational Protein Design with Application to the Development of a Biomolecular Tool-kit for Single Molecule Protein Sequencing. WUSTL. 2014;.
19. Tessler LA, Donahoe CD, Garcia DJ, Jun YS, Elbert DL, Mitra RD. Nanogel surface coatings for improved single-molecule imaging substrates. *Journal of The Royal Society Interface*. 2011; 8(63):1400–1408. <https://doi.org/10.1098/rsif.2010.0669>
20. Borgo B, Havranek JJ. Motif-directed redesign of enzyme specificity. *Protein Science*. 2014; 23(3):312–320. <https://doi.org/10.1002/pro.2417> PMID: 24407908
21. Mitra RD, Tessler LA. Single molecule protein screening; 2010. Available from: <http://www.google.com/patents/WO2010065531A1?cl=en>.
22. Sharonov A, Hochstrasser RM. Wide-field subdiffraction imaging by accumulated binding of diffusing probes. *Proceedings of the National Academy of Sciences*. 2006; 103(50):18911–18916. <https://doi.org/10.1073/pnas.0609643104>
23. Jungmann R, Steinhauer C, Scheible M, Kuzyk A, Tinnefeld P, Simmel FC. Single-molecule kinetics and super-resolution microscopy by fluorescence imaging of transient binding on DNA origami. *Nano letters*. 2010; 10(11):4756–4761. <https://doi.org/10.1021/nl103427w> PMID: 20957983
24. Swaminathan J, Boulgakov AA, Hernandez ET, Bardo AM, Bachman JL, Marotta J, et al. Highly parallel single-molecule identification of proteins in zeptomole-scale mixtures. *Nature biotechnology*. 2018; 36(11):1076. <https://doi.org/10.1038/nbt.4278>
25. Tessler LA, Mitra RD. Sensitive single-molecule protein quantification and protein complex detection in a microarray format. *Proteomics*. 2011; 11(24):4731–4735. <https://doi.org/10.1002/pmic.201100361> PMID: 22038904
26. Chandradoss SD, Haagsma AC, Lee YK, Hwang JH, Nam JM, Joo C. Surface passivation for single-molecule protein studies. *Journal of visualized experiments: JoVE*. 2014;(86). <https://doi.org/10.3791/50549> PMID: 24797261
27. Selvin PR, Ha T. *Single-molecule techniques*. Cold Spring Harbor Laboratory Press; 2008.
28. Joo C, Fareh M, Kim VN. Bringing single-molecule spectroscopy to macromolecular protein complexes. *Trends in biochemical sciences*. 2013; 38(1):30–37. <https://doi.org/10.1016/j.tibs.2012.10.005> PMID: 23200186
29. Groll J, Moeller M. Star polymer surface passivation for single-molecule detection. In: *Methods in enzymology*. vol. 472. Elsevier; 2010. p. 1–18.
30. Finkelstein IJ, Greene EC. Supported lipid bilayers and DNA curtains for high-throughput single-molecule studies. In: *DNA Recombination*. Springer; 2011. p. 447–461.
31. Pan H, Xia Y, Qin M, Cao Y, Wang W. A simple procedure to improve the surface passivation for single molecule fluorescence studies. *Physical biology*. 2015; 12(4):045006. <https://doi.org/10.1088/1478-3975/12/4/045006> PMID: 26118480
32. Edman P, et al. Method for determination of the amino acid sequence in peptides. *Acta chem scand*. 1950; 4(7):283–293. <https://doi.org/10.3891/acta.chem.scand.04-0283>
33. Laursen RA. Solid-Phase Edman Degradation. *The FEBS Journal*. 1971; 20(1):89–102.
34. Vogelsang J, Kasper R, Steinhauer C, Person B, Heilemann M, Sauer M, et al. A reducing and oxidizing system minimizes photobleaching and blinking of fluorescent dyes. *Angewandte Chemie International Edition*. 2008; 47(29):5465–5469. <https://doi.org/10.1002/anie.200801518> PMID: 18601270
35. Pennacchietti F, Gould TJ, Hess ST. The role of probe photophysics in localization-based superresolution microscopy. *Biophysical journal*. 2017; 113(9):2037–2054. <https://doi.org/10.1016/j.bpj.2017.08.054> PMID: 29117527
36. Schlau-Cohen GS, Wang Q, Southall J, Cogdell RJ, Moerner W. Single-molecule spectroscopy reveals photosynthetic LH2 complexes switch between emissive states. *Proceedings of the National Academy of Sciences*. 2013; 110(27):10899–10903. <https://doi.org/10.1073/pnas.1310222110>

37. van Oijen AM. Single-molecule approaches to characterizing kinetics of biomolecular interactions. *Current opinion in biotechnology*. 2011; 22(1):75–80. <https://doi.org/10.1016/j.copbio.2010.10.002> PMID: 21036593
38. Foote J, Eisen HN. Kinetic and affinity limits on antibodies produced during immune responses. *Proceedings of the National Academy of Sciences of the United States of America*. 1995; 92(5):1254. <https://doi.org/10.1073/pnas.92.5.1254> PMID: 7877964
39. Nemoto N, Miyamoto-Sato E, Yanagawa H. Fluorescence labeling of the C-terminus of proteins with a puromycin analogue in cell-free translation systems. *FEBS letters*. 1999; 462(1):43–46. [https://doi.org/10.1016/S0014-5793\(99\)01474-X](https://doi.org/10.1016/S0014-5793(99)01474-X) PMID: 10580088
40. Xu G, Shin SBY, Jaffrey SR. Chemoenzymatic labeling of protein C-termini for positive selection of C-terminal peptides. *ACS chemical biology*. 2011; 6(10):1015–1020. <https://doi.org/10.1021/cb200164h> PMID: 21812462
41. Lu Y, Lee Bh, King RW, Finley D, Kirschner MW. Substrate degradation by the proteasome: a single-molecule kinetic analysis. *Science*. 2015; 348(6231):1250834. <https://doi.org/10.1126/science.1250834> PMID: 25859050
42. Dempsey GT, Vaughan JC, Chen KH, Bates M, Zhuang X. Evaluation of fluorophores for optimal performance in localization-based super-resolution imaging. *Nature methods*. 2011; 8(12):1027–1036. <https://doi.org/10.1038/nmeth.1768> PMID: 22056676
43. Cui Y, Wei Q, Park H, Lieber CM. Nanowire nanosensors for highly sensitive and selective detection of biological and chemical species. *Science*. 2001; 293(5533):1289–1292. <https://doi.org/10.1126/science.1062711> PMID: 11509722
44. Patolsky F, Zheng G, Hayden O, Lakadamyali M, Zhuang X, Lieber CM. Electrical detection of single viruses. *Proceedings of the National Academy of Sciences of the United States of America*. 2004; 101(39):14017–14022. <https://doi.org/10.1073/pnas.0406159101> PMID: 15365183
45. Stern E, Klemic JF, Routenberg DA, Wyrembak PN, Turner-Evans DB, Hamilton AD, et al. Label-free immunodetection with CMOS-compatible semiconducting nanowires. *Nature*. 2007; 445(7127):519–522. <https://doi.org/10.1038/nature05498> PMID: 17268465
46. Kim A, Ah CS, Yu HY, Yang JH, Baek IB, Ahn CG, et al. Ultrasensitive, label-free, and real-time immunodetection using silicon field-effect transistors. *Applied Physics Letters*. 2007; 91(10):103901–103901. <https://doi.org/10.1063/1.2779965>
47. Rothberg JM, Hinz W, Rearick TM, Schultz J, Mileski W, Davey M, et al. An integrated semiconductor device enabling non-optical genome sequencing. *Nature*. 2011; 475(7356):348–352. <https://doi.org/10.1038/nature10242> PMID: 21776081
48. Bellin DL, Warren SB, Rosenstein JK, Shepard KL. Interfacing CMOS electronics to biological systems: from single molecules to cellular communities. In: *Biomedical Circuits and Systems Conference (BioCAS)*, 2014 IEEE. IEEE; 2014. p. 476–479.
49. Sorgenfrei S, Chiu Cy, Gonzalez RL Jr, Yu YJ, Kim P, Nuckolls C, et al. Label-free single-molecule detection of DNA-hybridization kinetics with a carbon nanotube field-effect transistor. *Nature nanotechnology*. 2011; 6(2):126–132. <https://doi.org/10.1038/nnano.2010.275> PMID: 21258331
50. Lu N, Dai P, Gao A, Valiaho J, Kallio P, Wang Y, et al. Label-Free and Rapid Electrical Detection of hTSH with CMOS-Compatible Silicon Nanowire Transistor Arrays. *ACS applied materials & interfaces*. 2014; 6(22):20378–20384. <https://doi.org/10.1021/am505915y>
51. Guo N, Cheung KW, Wong HT, Ho D. CMOS Time-Resolved, Contact, and Multispectral Fluorescence Imaging for DNA Molecular Diagnostics. *Sensors*. 2014; 14(11):20602–20619. <https://doi.org/10.3390/s141120602> PMID: 25365460